

Identification of Nonlinear Elastic Bending Behavior for Cable Simulation

Tian Zhao^{1,2}, Fabio Schneider-Jung¹, Joachim Linn¹, Ralf Müller²

¹ Department of Mathematics for Vehicle Engineering
Fraunhofer Institute for Industrial Mathematics ITWM
Fraunhofer-Platz 1, 67663 Kaiserslautern, Germany
[tian.zhao, fabio.julian.schneider-jung, joachim.linn]@itwm.fraunhofer.de

² Department of Civil and Environmental Engineering
Technical University of Darmstadt
Franziska-Braun-Straße 7, 64287 Darmstadt, Germany
ralf.mueller@mechanik.tu-darmstadt.de

ABSTRACT

This paper investigates the identification of nonlinear elastic behavior of real cables, namely a bending stiffness characteristic, based on real cable experiments. To this end, two approaches are considered: a data-based approach, where an inverse problem is formulated, and a model-based approach, utilizing the static equilibrium equations for Cosserat rods. Both methods are applied to measured data of real cables, and the obtained results are compared and discussed. Our proposed methods contribute to the development of realistic constitutive models for cable simulation within the framework of nonlinear rod models.

Keywords: Cable simulation, Nonlinear elasticity.

1 INTRODUCTION

Flexible slender structures, such as cables and hoses, are widely used in the automotive industry. As a result, there is an increasing demand for simulation tools to simulate their mechanical behavior realistically and efficiently. Typical applications of such a simulation tool are illustrated in [1] and [2].

Cosserat rod theory provides a suitable framework for efficient and geometrically exact modeling to simulate slender flexible structures. As outlined in [2], static equilibrium states of elastic Cosserat rods can be obtained by minimizing their potential energy, which comprises the external potential and elastic energy. In [2], as likewise in more or less all publications on Cosserat rod models, a linear constitutive law is used to formulate the elastic energy of the rod. However, nonlinear elastic behavior, observed in cyclic pure bending [3] and MeSOMICS bending experiments [4], may play a significant role in complex structures.

In our recent study [5], based on the framework proposed in [2], we developed an iterative method to incorporate nonlinear elastic behavior. In each iteration, the local bending stiffness constants are updated, based on a given characteristic, the new equilibrium state is computed by energy minimization, and we iterate until the cable state converges. The results of our study were promising, as they enabled efficient and correct simulations with nonlinear elastic bending behavior.

In this work, we focus on the identification of nonlinear elastic constitutive bending behavior, which then can be used in the iterative method. Already in [5], we formulated an inverse problem to determine the nonlinear elastic properties, i.e. a state-dependent bending stiffness characteristic for given measurement data.

We continue our work of identifying the bending stiffness characteristics of cables by proposing enhancements of the inverse problem, where pre-curvature is considered as additional optimization variable. Moreover, we investigate an alternative method (besides the inverse problem) which is based on the static equilibrium equations for Cosserat rods.

The paper is structured as follows: In Section 2, we briefly sketch our iterative method for simulating nonlinear elastic behavior. Section 3 introduces the real- and virtual bending experiments. In section 4, we present the inverse problem and show how considering pre-curvature as an additional optimization variable enhances the results. Section 5 presents the alternative method for determining the nonlinear elasticity based on the static equilibrium equations for Cosserat rods. Finally, in Section 6, we present a conclusion of our work.

2 ITERATIVE METHOD TO SIMULATE NONLINEAR ELASTIC BEHAVIOR

In this section, we briefly sketch the iterative method proposed in [5], which enables the simulation of nonlinear elastic bending behavior for a Cosserat rod.

2.1 Cosserat rod in two-dimensional space

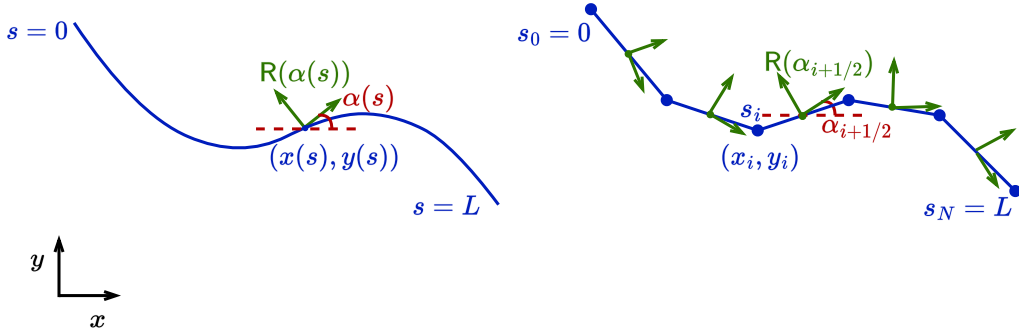


Figure 1: Left: Continuous Cosserat rod in \mathbb{R}^2 . Right: Discrete Cosserat rod in \mathbb{R}^2 .

We consider a Cosserat rod in two-dimensional space to simulate the bending deformation in the $x - y$ plane (see Fig. 1). The Cosserat rod is described by the centerline $(x(s), y(s))^T \in \mathbb{R}^2$ and the rotation angle $\alpha(s)$ parametrizing the local frame

$$R(s) = \begin{pmatrix} \cos(\alpha(s)) & -\sin(\alpha(s)) \\ \sin(\alpha(s)) & \cos(\alpha(s)) \end{pmatrix}, \quad (1)$$

with curve parameter $s \in [0, L]$ measuring the arc length of the centerline in the reference configuration of the rod.

The curvature of the moving frame, which approximately corresponds to the curvature of the centerline, and the material tangent vector containing the components of the centerline tangent vector w.r.t the local frame, are given as

$$K(s) = \alpha'(s) \quad \text{and} \quad \mathbf{\Gamma}(s) = \begin{pmatrix} \Gamma_1(s) \\ \Gamma_2(s) \end{pmatrix} = R(s)^T \cdot \begin{pmatrix} x(s) \\ y(s) \end{pmatrix}', \quad (2)$$

where the difference functions $\Delta K(s) = K(s) - K_0(s)$ and $\Delta \mathbf{\Gamma}(s) = \mathbf{\Gamma}(s) - \mathbf{\Gamma}_0(s)$ represent the deviation of $K(s)$ and $\mathbf{\Gamma}(s)$ from reference values $K_0(s)$ and $\mathbf{\Gamma}_0 = (1, 0)^T$.

2.2 Minimization of potential energy

For the case of linear elastic constitutive behavior, the elastic potential energy of the Cosserat rod is given as

$$W = \frac{1}{2} \int_0^L \Delta \mathbf{\Gamma}^T(s) \cdot \mathbf{C}_\Gamma \cdot \Delta \mathbf{\Gamma}(s) ds + \frac{1}{2} \int_0^L [EI] \cdot \Delta K(s)^2 ds, \quad (3)$$

where the first term represents the shear and tension energy, and the second term represents the bending energy. The coefficient matrix $C_{\Gamma} = \begin{pmatrix} [EA] & 0 \\ 0 & [GA] \end{pmatrix}$ contains the effective tension stiffness $[EA]$ as well as effective shear stiffness $[GA]$, and $[EI]$ is the effective bending stiffness.

The discrete counterpart can be written as

$$V = \frac{1}{2} \sum_{i=0}^{N-1} \Delta s_{i+1/2} \cdot (\Delta \Gamma_{i+1/2})^T \cdot C_{\Gamma} \cdot \Delta \Gamma_{i+1/2} + \frac{1}{2} \sum_{i=0}^N \delta s_i \cdot [EI] \cdot \Delta K_i^2, \quad (4)$$

where the index i denotes vertex quantities at s_i for $i = 0, \dots, N$ and $i + 1/2$ denotes edge-centered quantities at $s_{i+1/2}$ for $i = 0, \dots, N - 1$. Further details about the derivation from continuous case can be found in [2].

The static equilibrium of the rod under given boundary conditions can be obtained in an efficient and robust way by minimizing its potential energy [2].

Since we want to enable nonlinear elastic bending behavior, we introduce a state-dependent (or more precisely, curvature-dependent) bending stiffness characteristic $f_{EI}(\kappa)$, as already suggested in [5]. With this, we rewrite the bending energy term to

$$V_{B,nl} = \frac{1}{2} \sum_{i=0}^N \delta s_i \int_{K_{0,i}}^{K_i} \int_{K_{0,i}}^{\xi} f_{EI}(\kappa) d\kappa d\xi, \quad (5)$$

which for $f_{EI}(\kappa) = [EI] = \text{const.}$ equals the bending energy term in (4).

In principle, one could solve the energy minimization problem with $V_{B,nl}$ as bending energy term. However, directly solving the energy minimization problem in this more general form is computationally expensive.

2.3 Iterative update of bending stiffness

In order to maintain the efficiency of the energy minimization problem for the linear elastic case, we proposed an iterative method where in each step we only consider an energy formulation as in (4). This can be achieved by iterative updates of local bending stiffness constants, depending on the current local curvature and the given bending stiffness characteristic according to the algorithmic procedure suggested in [5]:

In the m th iteration step, a given cable state (x_i^m, y_i^m) , $i = 0, \dots, N$ and $\alpha_{i+1/2}^m$, $i = 0, \dots, N - 1$, provides corresponding curvatures K_i^m such that we can update the constant local bending stiffness at each vertex according to the given bending stiffness characteristic. Minimizing the potential energy leads to a new equilibrium state (x_i^{m+1}, y_i^{m+1}) , $\alpha_{i+1/2}^{m+1}$ and corresponding curvatures K_i^{m+1} . This process is performed iteratively until the cable state converges.

3 BENDING EXPERIMENT

We perform real as well as virtual bending experiments to study the bending behavior of cables. The real experiments are performed on the MeSOMICS measurement machine [4].

3.1 Real bending experiment

In the real bending experiment (cf. Fig. 2), the specimen is mounted between two low-friction bearings, such that we have (ideally) moment-free boundary conditions at both clamping points. To create various bending deformations, the left clamping point is displaced stepwise towards the right clamping point while measuring the resulting reaction force at the right clamping point. Moreover, for each configuration, a camera captures the bending deformation and the cable centerline line is detected.

Fig. 2 displays top-view pictures of a cable with length $L = 181$ mm and diameter $d = 4.6$ mm. The three images in Fig. 2 depict cable configurations (a), (b) and (c) with applied displacements of d , $2d$ and $3d$ respectively.

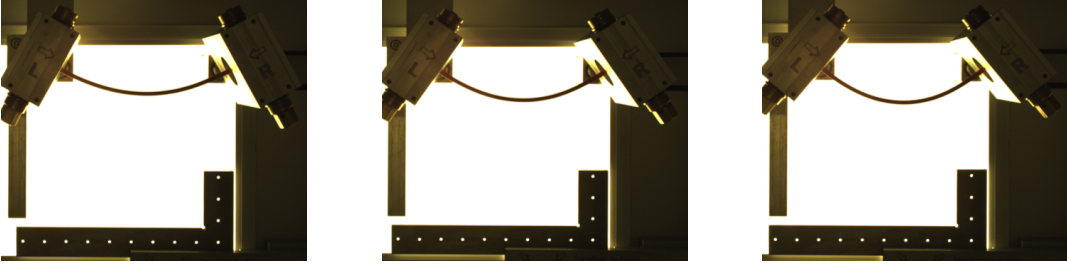


Figure 2: Top-view of real bending experiment. Left: Cable configuration (a), with applied displacement d . Middle: Cable configuration (b), with applied displacement $2d$. Right: Cable configuration (c), with applied displacement $3d$.

3.2 Virtual bending experiment

In addition to real bending experiments, we also perform virtual bending experiments using the iterative method from Section 2. The boundary conditions for the virtual experiment are the same as those used for the real experiment, and we virtually measure the resulting forces for the applied boundary conditions. Fig. 3 shows an example of the bending deformations in virtual bending experiment.

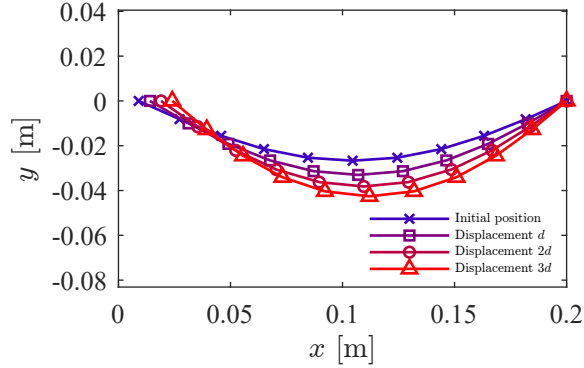


Figure 3: Bending deformations of the initial rod (already slightly bent) and three displacement steps d , $2d$, $3d$, with $d = 5 \cdot 10^{-3}$ m.

4 INVERSE PROBLEM

In this work, we focus on the question how to determine the nonlinear elastic behavior from given measurement results. In our previous work [5], we already formulated an inverse problem, where we aimed to find the bending stiffness characteristic which leads to a simulated reaction force that closely matches the measured target force.

More concretely, we formulate the problem as finding $f_{EI}(\kappa)$ such that

$$l = \sum_{j=1}^J (F_j^S - F_j^G)^2 < tol, \quad (6)$$

where the index $j = 1, \dots, J$ denotes the given displacements, F_j^S represents the simulated force computed from the current $f_{EI}(\kappa)$ at displacement step j and F_j^G represents the corresponding measured target force.

Here, the state-dependent bending stiffness characteristic is modeled using a natural cubic spline with three control points, denoted by $(\hat{\kappa}_0, [\hat{EI}]_0)$, $(\hat{\kappa}_1, [\hat{EI}]_1)$ and $(\hat{\kappa}_2, [\hat{EI}]_2)$. Thus, a rather small number of control points represent the unknowns of the inverse problem. For simplicity, we even assume fixed $\hat{\kappa}_0$, $\hat{\kappa}_1$ and $\hat{\kappa}_2$ and only consider $[\hat{EI}]_0$, $[\hat{EI}]_1$ and $[\hat{EI}]_2$ as optimization variables. The optimization is achieved by a Levenberg-Marquardt method in MATLAB [6].

From the preliminary results presented in [5] we concluded that it is necessary to add pre-curvature to the set of optimization variables, as the cable specimens in practice are slightly bent rather than perfectly straight, and we found that pre-curvature significantly influences the optimization results.

In principle, the pre-curvature $K_0(s)$ could vary along the rod. But here, for simplicity and since for our purpose it sufficiently approximates the reality, we only consider a constant \hat{K}_0 .

As the set of optimization variables was extended, we also augmented the objective function \hat{l} in Equation (6) by an additional term, measuring the difference between simulated and optically detected curvature

$$\hat{l} = \sum_{j=1}^J (F_j^S - F_j^G)^2 + w \cdot \sum_{j=1}^J \sum_{i=0}^N (K_{j,i}^S - K_{j,i}^G)^2 < tol, \quad (7)$$

where w is a weighting factor (set to $w = 10^{-3}$) for the curvature term, $K_{j,i}^S$ are the simulated curvatures and $K_{j,i}^G$ are the corresponding measured target curvatures. The index j denotes, as for the forces, the given displacements, while the index i indicates the arc length positions s_i .

4.1 Inverse problem using virtual measurement data

In order to verify the solution of the inverse problem, virtual measurement data is used. This means, we simulate the force F_j^G for $j = 1, \dots, J$ for a known state-dependent bending stiffness characteristic $f_{EI}(\kappa)$ and a known pre-curvature \hat{K}_0 . Thus, we can compare the solution of the inverse problem, i.e. the identified bending stiffness characteristic and pre-curvature, with the ones used to generate the virtual measurement data. The used model parameters are shown in Table 1.

parameter	d	L	$\hat{\kappa}_0$	$\hat{\kappa}_1$	$\hat{\kappa}_2$	$[\hat{EI}]_0$	$[\hat{EI}]_1$	$[\hat{EI}]_2$	\hat{K}_0
unit	[m]	[m]	[m ⁻¹]	[m ⁻¹]	[m ⁻¹]	[Nm ²]	[Nm ²]	[Nm ²]	[m ⁻¹]
value	$5 \cdot 10^{-3}$	0.2	0	5	10	$5 \cdot 10^{-3}$	$3 \cdot 10^{-3}$	$2 \cdot 10^{-3}$	2

Table 1: Model parameters for virtual bending experiment.

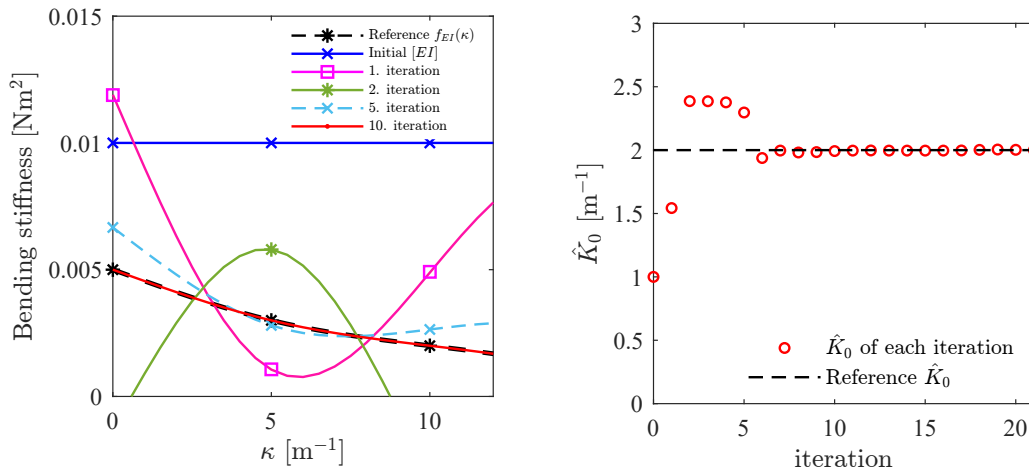


Figure 4: Evolution of $f_{EI}(\kappa)$ (left) and \hat{K}_0 (right) during optimization.

The optimization process used to determine the $f_{EI}(\kappa)$ and the pre-curvature \hat{K}_0 is illustrated in Fig. 4. The procedure starts with a constant bending stiffness ($[EI] = 0.01 \text{ Nm}^2$), and iteratively approaches the reference $f_{EI}(\kappa)$ (plotted as black dashed line in Fig. 4 (left)), which was used to generate the virtual measurement data. By the 10th iteration, the optimization achieves good agreement with the reference $f_{EI}(\kappa)$. Subsequent iteration steps produce almost the same output. The right plot of Fig. 4 illustrates the evolution of the pre-curvature \hat{K}_0 during the optimization process. Starting with an initial value 1 m^{-1} , also \hat{K}_0 approaches its reference value (black dashed line) after approx. 10 iterations.

Furthermore, the quantities in the objective function, i.e. the simulated force F_j^S and curvature $K_{j,i}^S$, are shown in Fig. 5. In the left plot, the evolution of forces during optimization is visualized, while in the right plot the local curvatures are plotted. Here, only the local curvatures of the maximum deformation (i.e. configuration (c) with applied displacement $3d$) are shown. Again, after 10 iterations the simulated quantities nicely coincide with their reference values.

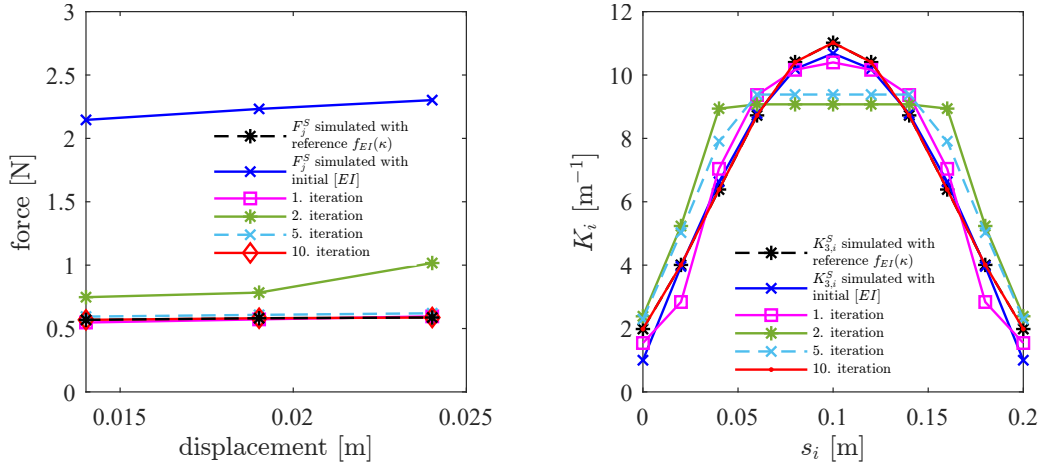


Figure 5: Left: Simulated forces F_j^S during optimization. Right: Simulated curvatures $K_{j,i}^S$ for configuration (c) with displacement $3d$ during optimization.

Summarizing, the above considerations with virtual measurement data show that solving the inverse problem leads to the correct bending stiffness characteristic and pre-curvature.

4.2 Inverse problem using real measurement data

In the previous section, we illustrated the feasibility of our optimization approach to solve the inverse problem, utilizing virtual measurement data. Now, we want to identify the bending stiffness characteristic and pre-curvature of a real cable. To this end, the inverse problem is applied to measured reaction forces and optically detected curvature of the cable. The measured reaction force is plotted in the right plot of Fig. 6 (dashed black line). The cable configurations from which the curvature is detected are shown in Fig. 2.

The identified bending stiffness characteristic is visualized in the left plot of Fig. 6. The red solid line shows the solution of the enhanced inverse problem, i.e. with \hat{K}_0 as optimization variable. For comparison, we also added the resulting bending stiffness characteristic when pre-curvature is simply set to zero and is not considered as optimization variable (black dashed line). The latter suffers from nonphysical (negative) values for low curvatures.

However, the corresponding simulated forces (red and green dashed lines in the right plot of Fig. 6) only show small deviations, from both the reference force and from each other. This illustrates the necessity consider pre-curvature in the optimization.

In total, also for real cables and corresponding measurement data, the inverse problem provides physically plausible bending stiffness characteristics, which can be used in the iterative method

presented in Section 2.

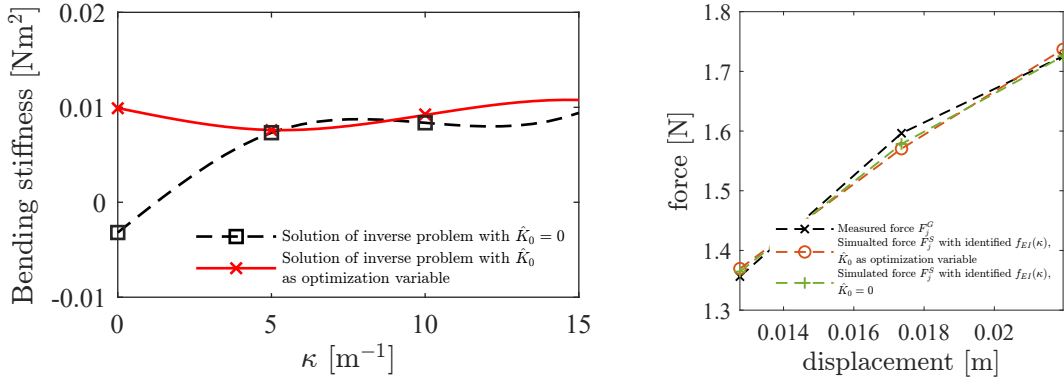


Figure 6: Left: Identified bending stiffness characteristic (with set $\hat{K}_0 = 0$ and \hat{K}_0 as optimization variable) for a real cable. Right: Measured and simulated force (orange: with solid red characteristic and identified \hat{K}_0 ; green: with dashed black characteristic and $\hat{K}_0 = 0$).

5 BALANCE EQUATIONS AND $(\kappa, f_{EI}(\kappa))$ -GRAPH

To assess the results of the inverse problem, we investigate an alternative approach to identify the bending stiffness characteristic, which is based on the balance equations for a Cosserat rod. Thus, besides the data-driven inverse problem, we also investigate a model-based approach.

In the absence of external body forces and moments acting on the Cosserat rod, the equilibrium equations are given by

$$\partial_s \mathbf{f} = \mathbf{0}, \quad (8)$$

$$\partial_s \mathbf{m} + \partial_s \boldsymbol{\varphi} \times \mathbf{f}(s) = \mathbf{0}, \quad (9)$$

where $\boldsymbol{\varphi}(s) = (x(s), y(s), z(s))^T \in \mathbb{R}^3$ is the centerline of the rod, $\mathbf{f}(s) = (f^x(s), f^y(s), f^z(s))^T \in \mathbb{R}^3$ is the force vector, and $\mathbf{m}(s) = (m^x(s), m^y(s), m^z(s))^T \in \mathbb{R}^3$ is the moment vector. According to the derivation given by Simo [7], Equations (8) and (9) hold independent of any assumptions on the constitutive behavior of the rod, and the considerations in [8] point out that they also hold independent of internal kinematic constraints that enforce inextensibility of the rod or inhibit transverse shearing of its cross sections.

Integrating Equations (8) and (9) leads to

$$\mathbf{f}(s) = \mathbf{f}, \quad (10)$$

$$\mathbf{m}(s) + \boldsymbol{\varphi}(s) \times \mathbf{f} = \mathcal{M}, \quad (11)$$

with constants \mathbf{f} and \mathcal{M} along the rod.

In two dimensional space, it holds $\boldsymbol{\varphi}(s) = (x(s), y(s), 0)^T$, $\mathbf{f}(s) = (f^x(s), f^y(s), 0)^T$, and $\mathbf{m}(s) = (0, 0, m(s))^T$. Thus, Equation (11) can be written as

$$m(s) + x(s) \cdot f^y - y(s) \cdot f^x = \mathcal{M}, \quad (12)$$

where \mathcal{M} is a constant scalar.

For our bending experiment (see Fig. 2), we have moment-free boundary conditions at both simply supported end points $m(0) = 0$ and $m(L) = 0$. Since the y -coordinates of both clamping points are equal and the left point only is displaced in x -direction, the resulting force in y -direction is vanishing, i.e. $f^y = 0$. By choosing the coordinate system such that $y(0) = 0$, we obtain $\mathcal{M} = 0$. Thus, the bending moment at arc length s is given by

$$m(s) = y(s) \cdot f^x. \quad (13)$$

Furthermore, we can calculate the curvature of the bending line using $K(s) = \frac{d\theta(s)}{ds}$, where $\theta(s) = \arctan(\frac{dy}{dx})$. The state-dependent bending stiffness for curvature $K(s)$ can be obtained by

$$\left. \frac{dm(\kappa)}{d\kappa} \right|_{\kappa=K(s)} =: f_{EI}(K(s)). \quad (14)$$

Summarizing, from measured forces as well as the optically detected bending line and corresponding curvature, we can generate a $(K(s), f_{EI}(K(s)))$ -graph. Since our bending experiment provides an interval of curvatures, with the curvature vanishing at the boundaries and reaching its maximum in the middle, we get a graph for each configuration.

5.1 Real measurement data

We compute the $(\kappa, f_{EI}(\kappa))$ -graphs for the real measurement data, which was already used for the inverse problem.

The $(K(s), f_{EI}(K(s)))$ -graphs for configuration (a), (b) and (c) (see Fig. 7 (left), corresponding to pictures in Fig. 2) are plotted in Fig. 7 (right). We observe good consistency among the three identified graphs, which could be combined to one bending stiffness characteristic. However, comparing the results with those from the inverse problem (the dashed orange line), we observe clear deviations. While the order of magnitude is similar, the qualitative behavior significantly differs. So far, we did not consider pre-curvature in the model-based approach, which might be one source for the discrepancies. To understand the source of deviations is topic of our current research.

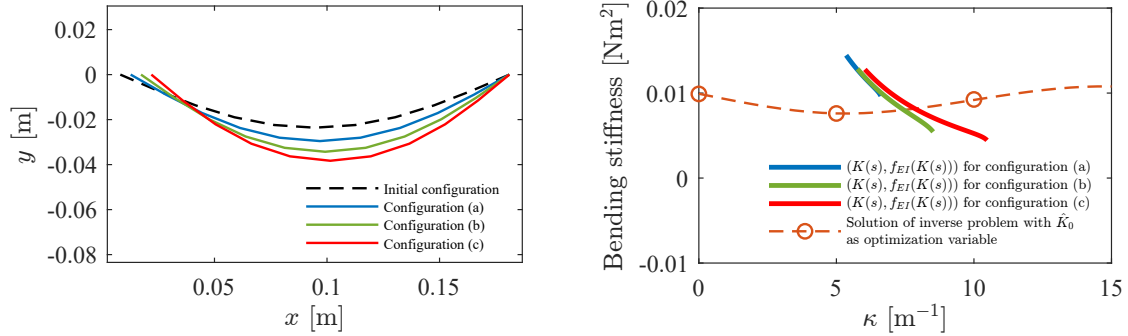


Figure 7: Left: Simulated bending configurations (a), (b) and (c). Right: $(K(s), f_{EI}(K(s)))$ -graphs determined by method based on balance equations, together with the $f_{EI}(\kappa)$ identified by inverse problem.

6 CONCLUSIONS

In summary, in this contribution, we continue our work on the simulation of nonlinear elastic bending behavior of real cables. While an efficient forward simulation already could be presented in our previous work [5], we now focus our work on a robust method to identify realistic stiffness characteristics for the nonlinear elastic bending behavior of cables, which is essential for reliable simulations. Although the inverse problem seems promising, we intend to assess the results by a more model-based approach, which is currently investigated.

ACKNOWLEDGMENTS

This work is part of the "BordNetzSim3D"-project (funding code: 19S21003C), funded by the German Federal Ministry for Economic Affairs and Climate Action.

Gefördert durch:



aufgrund eines Beschlusses
des Deutschen Bundestages

REFERENCES

- [1] Linn, J., Schneider, F., Dreßler, K., Hermanns, O.: Virtual product development and digital validation in automotive industry. In Bock, H.G., Küfer, K.H., Maass, P., Milde, A., Schulz, V., eds.: *German Success Stories in Industrial Mathematics*. Volume 35. Springer International Publishing, Cham (2021) 45–52 ISBN:978-3-030-81455-7.
- [2] Linn, J., Hermansson, T., Andersson, F., Schneider, F.: Kinetic aspects of discrete cosserat rods based on the difference geometry of framed curves. In Valasek, M., et al., eds.: *ECCOMAS Thematic Conference on Multibody Dynamics*, Prague, Czech Republic (2017) 163–176
- [3] Dörlich, V., Linn, J., Diebels, S.: Flexible beam-like structures - experimental investigation and modeling of cables. In Altenbach, H., Jablonski, F., Müller, W.H., Naumenko, K., Schneider, P., eds.: *Advances in Mechanics of Materials and Structural Analysis: In Honor of Reinhold Kienzler*. Volume 80. Springer International Publishing, Cham (2018) 27–46 doi:10.1007/978-3-319-70563-7_2.
- [4] MeSOMICS: Measurement system for the optically monitored identification of cable stiffnesses. Homepage: www.mesomics.eu
- [5] Zhao, T., Schneider-Jung, F.J., Linn, J., Müller, R.: Simulating nonlinear elastic behaviour of cables using an iterative method. In: *ECCOMAS Congress 2022-8th European Congress on Computational Methods in Applied Sciences and Engineering*. (2022) doi: 10.23967/eccomas.2022.246.
- [6] MATLAB: Matlab version: 9.12.0 (r2022a). The MathWorks Inc. Natick, Massachusetts, United States. <https://www.mathworks.com>.
- [7] Simo, J.: A finite strain beam formulation. the three-dimensional dynamic problem. part i. *Computer Methods in Applied Mechanics and Engineering* **49**(1) (1985) 55–70 doi: 10.1016/0045-7825(85)90050-7.
- [8] Chouaieb, N., Maddocks, J.H.: Kirchhoff's problem of helical equilibria of uniform rods. *Journal of Elasticity* **77** (2004) 221–247 doi:10.1007/s10659-005-0931-z.